

Modulation of multi-timescale compound Ca-NMDA-Na oscillations in pyramidal neuron by extracellular electric fields

Yaqin Fan(樊亚琴), Meili Lu(卢梅丽), and Xile Wei(魏熙乐)

Citation: Chin. Phys. B, 2026, 35 (**6**): 060508. DOI: 10.1088/1674-1056/ae0897
http://cpb.iphy.ac.cn; http://iopscience.iop.org/cpb

What follows is a list of articles you may be interested in

Color image encryption algorithm using a new four-dimensional hyperchaotic system

Bo Lin(林博), Min Liu(刘敏), and Guodong Ye(叶国栋)
Chin. Phys. B, 2026, 35 (**5**): 050502. DOI: 10.1088/1674-1056/ae0bff

Mutual annihilation of counter-rotating spiral waves induced by electric fields

Ying-Qi Liu(刘瑛琦), Yi-Peng Hu(胡义鹏), Qian-Ming Ding(丁钱铭), Ying Xie(谢盈), and Ya Jia(贾亚)
Chin. Phys. B, 2025, 34 (**12**): 120505. DOI: 10.1088/1674-1056/ae0561

A sound-sensitive neuron incorporating a memristive-ion channel

Xin-Lin Song(宋欣林), Ge Zhang(张鬲), and Fei-Fei Yang(杨飞飞)
Chin. Phys. B, 2025, 34 (**12**): 120502. DOI: 10.1088/1674-1056/ae0563

Dynamical behaviors of a multifunctional neural circuit

Xiao-Hong Gao(高晓红), Kai-Long Zhu(朱凯龙), and Fei-Fei Yang(杨飞飞)
Chin. Phys. B, 2025, 34 (**9**): 090503. DOI: 10.1088/1674-1056/ae001b

Current bifurcation, reversals and multiple mobility transitions of dipole in alternating electric fields

Wei Du(杜威), Kao Jia(贾考), Zhi-Long Shi(施志龙), and Lin-Ru Nie(聂林如)
Chin. Phys. B, 2023, 32 (**2**): 020505. DOI: 10.1088/1674-1056/ac7dbe

---

Modulation of multi-timescale compound Ca–NMDA–Na oscillations in pyramidal neuron by extracellular electric fields

Yaqin Fan(樊亚琴)[1], Meili Lu(卢梅丽)[2], and Xile Wei(魏熙乐)[3,†]

[1] *Academy of Medical Engineering and Translational Medicine, Tianjin University, Tianjin* 300072, *China*
[2] *School of Information Technology Engineering, Tianjin University of Technology and Education, Tianjin* 300222, *China*
[3] *Tianjin Key Laboratory of Process Measurement and Control, School of Electrical and Information Engineering, Tianjin University, Tianjin* 300072, *China*

(Received 17 July 2025; revised manuscript received 8 September 2025; accepted manuscript online 18 September 2025)

Evidence shows that there exist dendritic Ca^{2+}-spike-dependent and NMDA-spike-dependent multi-timescale compound oscillations in epileptiform activity, and the electric field (EF) plays a significant role in the propagation of compound oscillations. However, it is still unclear how the EF-induced spatial polarization modulates the interaction between dendritic Ca^{2+} oscillations and NMDA oscillations, and subsequently influences somatic Na^+ spikes. To address this issue, we built a biophysical pyramidal neuron model with complex dendritic morphology, which is capable of reproducing multi-timescale neuronal oscillations observed in epileptiform discharges. By investigating the EF stimulation thresholds for triggering dendritic Ca^{2+} and NMDA spikes as well as somatic Na^+ discharges, we found that the dendritic depolarization first activates dendritic Ca^{2+} oscillations, subsequently leading to the generation of dendritic NMDA oscillations, which together facilitate Na^+ spike generation by counteracting somatic hyperpolarization. Finally, we proposed a minimal three-compartment neuronal model that successfully reproduces the Ca–NMDA–Na compound oscillations. Through singular perturbation and bifurcation analysis, we demonstrated the modulatory influence of EF on multi-timescale neuronal compound oscillations. Additionally, our results indicate that the EF-induced depolarization at the apical dendrite causes the system equilibrium point to experience an invariant circle saddle-node bifurcation to trigger dendritic Ca^{2+} oscillations. These oscillations then drive the basal dendrite to generate dendritic NMDA oscillations by experiencing a subcritical Hopf bifurcation. In this case, the soma experiences a subcritical Hopf bifurcation to produce Na^+ spikes. These results provide valuable insights into the mechanisms underlying the generation of epileptiform discharges in the brain, which is helpful for developing therapeutic strategies for epilepsy.

Keywords: epileptiform discharge, electric field, dendritic Ca^{2+} spike, dendritic NMDA spike, multi timescale neuronal oscillations

PACS: 05.45.–a, 02.70.–c, 02.30.Oz

DOI: 10.1088/1674-1056/ae0897 **CSTR:** 32038.14.CPB.ae0897

1. Introduction

Epilepsy is a complex neurological disorder characterized by recurrent seizures, often accompanied by disturbances in consciousness and abnormal motor activity.[1] As a dynamic brain dysfunction, epilepsy not only affects the physical health of patients but also has profound impacts on their psychological and social well-being. Despite the development of over 30 anti-epileptic drugs, approximately one-third of patients remain resistant to these treatments and still experience persistent seizures.[2] A notable feature of epilepsy is the propagation of epileptiform discharges,[3] which include fast and slow waves with different propagation speeds. To provide an effective treatment strategy for epilepsy, it is crucial to explore how these epileptiform activities generate and propagate.

As the important relay unit, the neuron includes dendrites, soma, and axon, which play a crucial role in the transformation of spatiotemporal synaptic inputs into nonlinear somatic output.[4,5] There exist voltage-gated sodium and potassium channels in the soma and axon, which are responsible for the generation of action potentials at the single-cell level, namely the somatic Na^+ spike. It has been pointed out that the abnormal discharge activity of pyramidal neurons contributes to epileptiform discharges, which are widely believed to be caused by an imbalance between excitation and inhibition.[6–9] Due to the determining role of the somatic Na^+ spike in neuronal encoding, decades of research[6,10,11] have focused on the impact of sodium–potassium channel abnormalities on somatic discharge.

With the development of experimental techniques, an increasing number of studies[4,11,12] have shown that there are abundant active ionic channels distributed along dendrites. In particular, the activation of sodium and calcium channels and NMDA receptor channels on dendrites can lead to local dendritic spikes with different timescales. For example, dendritic Ca^{2+} spikes typically last on the order of hundreds of milliseconds, dendritic NMDA spikes generally last around 100 milliseconds, while dendritic Na^+ spikes are much faster, occurring on the scale of a few milliseconds. These dendritic spikes

†Corresponding author. E-mail: xilewei@tju.edu.cn

© 2026 Chinese Physical Society and IOP Publishing Ltd. All rights, including for text and data mining, AI training, and similar technologies, are reserved.

not only make the dendrites integrate the input signal superlinearly but also facilitate burst discharges by generating somatic plateau potentials. Furthermore, it has been pointed out that the multi-timescale dendritic spikes significantly improve the neuronal computational capacity.[13] Importantly, they play a crucial role in the generation of epileptiform discharges.[14–16] Sivakumar *et al.*[14] pointed out that abnormal NMDA receptors can lead to different types of epileptiform discharges. Cain *et al.*[15] found that dendritic Ca^{2+} activity during epileptiform discharges is more pronounced than in normal physiological states. In particular, Chiang *et al.*[16] showed that coexisting dendritic-NMDA-oscillation-dependent fast waves and dendritic-Ca^{2+}-oscillation-dependent slow waves are present in epileptiform discharges, and the initiation of the fast wave depends on the slow wave. These results suggest that exploring the interaction mechanism of multi-time-scale dendritic oscillations is helpful to reveal how epileptiform discharges are generated.

Besides, neuronal activity is closely related to the conductive medium in the extracellular space. Many studies have shown that both the electromagnetic stimulation applied in the brain[17–19] and the firing activity of neurons in the brain[16] can cause changes in the extracellular conductive medium, which results in the formation of extracellular EF. Particularly, Qiu *et al.*[20] directly proved that different EF intensities would make the epileptiform fast and slow waves propagate with different speeds. Generally, EF regulates neuronal activity by inducing spatial polarization along the somato-dendritic axis. It is pointed out that the somatic polarization could affect epileptiform discharge by changing the spiking time and pattern as well as the action potential threshold.[21,22] More and more evidence[23–25] showed that dendritic polarization also plays an important role in regulating the somatic output by affecting the dendritic NMDA and Ca^{2+} spike. However, it is still unclear how the EF-induced spatial polarization affects the interaction among somatic Na^+ oscillation, dendritic NMDA and Ca^{2+} oscillation.

Electrophysiological experiments are the most direct way to investigate; however, the timescale of dendritic oscillations is several times higher than that of somatic Na^+ oscillations, and current detection methods are insufficient. Computational models, including single-compartment models, multi-compartment models, and complex morphology realistic neuron models, overcome the ethical limitations of clinical and physiological experiments, offering a powerful tool for researchers to explore how cellular-level changes affect the generation of neuronal epileptiform discharges. For example, our previous study[26] characterized the propagation of multi-timescale dendritic oscillations under EF stimulation and pointed out the respective contributions of dendritic NMDA and Ca^{2+} spikes. Further, we used a three-compartment model[27] to show how the multi-timescale dendritic oscillations interact with each other from a dynamical point of view, and pointed out that abnormal NMDA receptors lead to pathological compound oscillations. However, there is currently a lack of a computational model that characterizes the interactions of multi-timescale neuronal oscillations in response to EF stimulation.

Thus, to answer the above question, we first built a realistic neuronal model with complex dendritic morphology, which can simultaneously address the multi-timescale interactions among dendritic NMDA and Ca^{2+} oscillations as well as somatic Na^+ firing behaviors under EF stimulation. Then we explored the EF stimulation threshold for triggering dendritic NMDA and Ca^{2+} oscillations as well as somatic action potentials. Our results show that due to the different activation characteristics of gating variables, the EF stimulation thresholds for the three types of discharges (Ca^{2+}, NMDA, and Na^+) increase sequentially. Under the influence of the EF, the slower-scale Ca^{2+} oscillations are more likely to be activated first, serving as the oscillation "source" that can induce faster-scale NMDA oscillations, together leading to the generation of the fastest Na^+ discharges. Thus, the multi-timescale compound oscillations appear. Finally, to explore the EF-regulated dynamic mechanism, a minimal field effect model was built. Using singular perturbation theory and bifurcation dynamics analysis, we validated the regulatory mechanism of electric fields on multi-timescale compound oscillations. Furthermore, we found that the generation of dendritic Ca^{2+} oscillations experiences invariant circle saddle-node bifurcation, and dendritic NMDA oscillations and somatic Na^+ spikes would experience subcritical Hopf bifurcation. These insights gained from our research not only advance our understanding of how epileptiform activities are generated but also are helpful for developing therapeutic strategies for epilepsy.

2. Models and method

2.1. A biophysical model with complex dendritic morphology

Milton *et al.*[10] and Chiang *et al.*[16] found that there exist multi-timescale neuronal compound oscillations in pyramidal neurons during epileptiform discharges. These oscillations include slowest dendritic Ca^{2+}-mediated oscillations, slower dendritic NMDA-mediated oscillations, and fastest somatic Na^+ oscillations. In particular, dendritic Ca^{2+} spikes occur on the order of several hundred milliseconds, while dendritic NMDA discharges take place on a timescale of approximately 100 milliseconds, and somatic Na^+ spikes are much faster, occurring on the order of a few milliseconds.[28] To simulate the compound oscillatory behavior observed in epileptiform discharges, we built a layer 5 pyramidal neuron model, as shown in Fig. 1. This model includes one soma, one axon, 70 basal dendrites, and 116 apical dendrites. To generate the compound oscillatory phenomena under electrophysiological conditions, we referred to the model parameters of LarKum *et al.*[29] and

Chiang *et al.*[16] Here we set the membrane resistivity, axial resistivity, and membrane capacitance to 20 kΩ·cm^2, 530 Ω·cm, and 1.2 μF/cm^2, respectively.

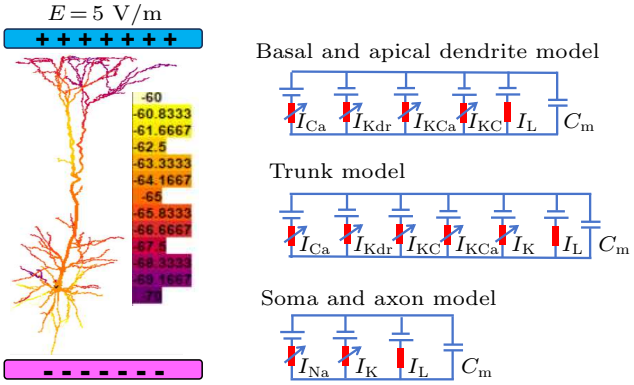


Fig. 1. Schematic diagram of the computational model of a layer 5 pyramidal neuron under EF stimulation. The model consists of a dendrite tree, a cell body, and an axon.

To generate action potentials in the soma and axon, the model includes HH-like sodium current (I_{Na}), HH-like potassium current (I_{K}), and passive leakage current (I_{L}). In the basal and apical dendrites, the following ionic currents are incorporated: calcium current (I_{Ca}), DR-type potassium current (I_{Kdr}), a long-duration Ca-dependent potassium current (I_{KCa}), a short-duration Ca^{2+}- and voltage-dependent potassium current (I_{KC}), and passive leakage current I_{L}. The dendritic trunk is modeled with I_{Ca}, I_{Kdr}, I_{KC}, I_{KCa}, I_{K}, and I_{L}. To generate dendritic Ca^{2+} spikes, we defined a "hot zone" located 500 μm from the soma, extending 300 μm toward the tuft region.[29] These ionic currents of the neuronal model are calculated using the following expressions:

$$
\begin{aligned}
&I_{\mathrm{Na}} = g_{\mathrm{Na}} m_{\mathrm{Na}}^3 h_{\mathrm{Na}} \left(V_{\mathrm{m}} - E_{\mathrm{Na}}\right), \quad I_{\mathrm{K}} = g_{\mathrm{K}} n_k^3 \left(V_{\mathrm{m}} - E_{\mathrm{K}}\right), \\
&I_{\mathrm{L}} = g_{\mathrm{L}} \left(V_{\mathrm{m}} - E_{\mathrm{L}}\right), \quad I_{\mathrm{Ca}} = g_{\mathrm{Ca}} m_{\mathrm{Ca}}^2 h_{\mathrm{Ca}} \left(V_{\mathrm{m}} - E_{\mathrm{Ca}}\right), \\
&I_{\mathrm{KC}} = g_{\mathrm{KC}} c \chi\left(Ca\right) \left(V_{\mathrm{m}} - E_{\mathrm{K}}\right), \quad I_{\mathrm{KCa}} = g_{\mathrm{KCa}} q \left(V_{\mathrm{m}} - E_{\mathrm{K}}\right), \\
&I_{\mathrm{Kdr}} = g_{\mathrm{Kdr}} n^4 \left(V_{\mathrm{m}} - E_{\mathrm{K}}\right),
\end{aligned} \tag{1}
$$

where V_{m} represents the membrane potential, $E_{\mathrm{Na}} = 50$ mV, $E_{\mathrm{K}} = -80$ mV, $E_{\mathrm{L}} = -70$ mV, and $E_{\mathrm{Ca}} = 30$ mV are the reversal potentials of the sodium channel, potassium channel, leaky channel, and calcium channel, respectively. g_{Na}, g_{K}, g_{L}, g_{Ca}, g_{KC}, g_{KCa}, and g_{Kdr} are the local conductance densities of I_{Na}, I_{K}, I_{L}, I_{Ca}, I_{KC}, I_{KCa}, and I_{Kdr}, respectively. The values of these conductance densities for different regions of the neuron are as follows:

Axon: $g_{\mathrm{Na}} = 30000$ pS/μm^2, $g_{\mathrm{K}} = 5000$ pS/μm^2; Soma: $g_{\mathrm{Na}} = 50$ pS/μm^2, $g_{\mathrm{K}} = 600$ pS/μm^2; the basal dendrites: $g_{\mathrm{L}} = 1$ pS/μm^2, $g_{\mathrm{Ca}} = 1.5$ pS/μm^2, $g_{\mathrm{KC}} = 100$ pS/μm^2, $g_{\mathrm{KCa}} = 10$ pS/μm^2, $g_{\mathrm{Kdr}} = 2500$ pS/μm^2; the trunk: $g_{\mathrm{K}} = 600$ pS/μm^2, $g_{\mathrm{L}} = 1$ pS/μm^2, $g_{\mathrm{Ca}} = 1$ pS/μm^2, $g_{\mathrm{KC}} = 80$ pS/μm^2, $g_{\mathrm{KCa}} = 1$ pS/μm^2, $g_{\mathrm{Kdr}} = 300$ pS/μm^2; the apical dendrite: $g_{\mathrm{L}} = 1$ pS/μm^2, $g_{\mathrm{Ca}} = 1.5$ pS/μm^2, $g_{\mathrm{KC}} = 80$ pS/μm^2, $g_{\mathrm{KCa}} = 10$ pS/μm^2, $g_{\mathrm{Kdr}} = 2$ pS/μm^2. The hot zone (located 500 μm from the soma, extending 300 μm toward the tuft region): $g_{\mathrm{L}} = 1$ pS/μm^2, $g_{\mathrm{Ca}} = 10$ pS/μm^2, $g_{\mathrm{KC}} = 80$ pS/μm^2, $g_{\mathrm{KCa}} = 10$ pS/μm^2, $g_{\mathrm{Kdr}} = 2$ pS/μm^2. It is important to note that, in order to generate dendritic Ca^{2+} oscillations, the conductance density g_{Ca} in the dendrites is multiplied by a factor *Cocai* relative to its initial state. Unless otherwise specified, $Cocai = 6.5$.

The dynamic expressions of gating variables for I_{Na}, I_{K}, I_{Ca}, and I_{KC} were as follows:

$$
\mathrm{d}x/\mathrm{d}t = \left(x_\infty - x\right)/\tau_x, \tag{2}
$$

where x_∞ and τ_x respectively represent the steady-state value and time constant, as shown in Table 1.

Table 1. Steady-state function and time constant of gating variables for layer 5 pyramidal neuron.

Gating varabile	Steady-state function	Time constant
m_{Na}	$m_{\mathrm{Na},\infty} = 1/\left(1 + \mathrm{e}^{\left((V_{\mathrm{m}}+55)/3\right)}\right)$	$\tau_{h_{\mathrm{Na}}} = 0.5$
n_{K}	$n_{\mathrm{K},\infty} = 1/\left(1 + \mathrm{e}^{\left(-(V_{\mathrm{m}}+50)/3\right)}\right)$	$\tau_{n_{\mathrm{K}}} = 1$
m_{Ca}	$m_{\mathrm{Ca},\infty} = 1/\left(1 + \mathrm{e}^{\left(-(V_{\mathrm{m}}+20)/16\right)}\right)$	$\tau_{\mathrm{mCa}} = 35$
h_{Ca}	$h_{\mathrm{Ca},\infty} = 1/\left(1 + \mathrm{e}^{\left((V_{\mathrm{m}}+40)/7\right)}\right)$	$\tau_{h_{\mathrm{Ca}}} = 157$
c	$c_\infty = 1/\left(1 + \mathrm{e}^{\left(-(V_{\mathrm{m}}+37)/7.2\right)}\right)$	$\tau_c = 20$

The dynamics of calcium concentration in the model can be depicted as follows:

$$
\frac{\mathrm{d}\left[\mathrm{Ca}^{2+}\right]_i}{\mathrm{d}t} = -v I_{\mathrm{Ca}} - \left[\mathrm{Ca}^{2+}\right]_i / \tau_{[Ca]}, \tag{3}
$$

where $v = 0.13$ cm^2/(ms·μA) and $\tau_{[\mathrm{Ca}]} = 13$ ms. The variable $[\mathrm{Ca}^{2+}]_i$ in our model is dimensionless, and it is proportional to the Ca^{2+} concentration in a thin internal cylindrical shell adjacent to the membrane. The $[\mathrm{Ca}^{2+}]_i$-dependent gate variable $\chi\left(\mathrm{Ca}\right)$ is characterized as follows:

$$
\chi\left(\mathrm{Ca}\right) = \frac{1}{1 + 6/\left[\mathrm{Ca}^{2+}\right]_i}. \tag{4}
$$

The gating variable q of I_{KCa} relies on its corresponding gate function:

$$
\frac{\mathrm{d}q}{\mathrm{d}t} = \frac{\left(q_\infty\left(\left[\mathrm{Ca}^{2+}\right]_i\right) - q\right)}{\tau_{\mathrm{q}}}, \tag{5}
$$

where $\tau_{\mathrm{q}} = 9$ ms, and the steady function q_∞ is depicted as follows:

$$
q_\infty\left(\left[\mathrm{Ca}^{2+}\right]_i\right) = \frac{1}{1 + 81/\left[\mathrm{Ca}^{2+}\right]_i^4}. \tag{6}
$$

The dynamic equation of the gating variable n of I_{Kdr} is characterized by

$$
\frac{\mathrm{d}n}{\mathrm{d}t} = \alpha_n\left(V_{\mathrm{m}}\right) - n\left(\alpha_n\left(V_{\mathrm{m}}\right) + \beta_n\left(V_{\mathrm{m}}\right)\right), \tag{7}
$$

where

$$
\alpha_n\left(V_{\mathrm{m}}\right) = \frac{0.00049\left(V_{\mathrm{m}} - 32\right)}{1 - \exp\left[\left(-\dfrac{V_{\mathrm{m}} - 32}{25}\right)\right]},
$$

$$\beta_n(V_{\rm m}) = \frac{0.00008\,(V_{\rm m}-42)}{\exp\left[\left(\dfrac{V_{\rm m}-42}{10}\right)\right]-1}. \quad (8)$$

In pyramidal neurons, NMDA receptors are typically distributed across the basal, oblique, and apical dendrites. To distinguish dendritic NMDA oscillations from dendritic Ca^{2+} oscillations, NMDA receptors in this model are specifically distributed at the basal dendrites, positioned 100 μm from the branch endpoints.[30] The dynamics of NMDA synaptic currents are depicted by the following equation:

$$I_{\rm NMDA}(t) = g_{\rm NM}(E_{\rm NMDA}-V_{\rm m})/\left(1+0.3\,{\rm e}^{-0.08V_{\rm m}}\right), \quad (9)$$

where $E_{\rm NMDA}=0$ represents the reversal potential of NMDA synaptic inputs, and $g_{\rm NM}$ denotes the conductance of synaptic currents. As outlined in our previous study,[16] $g_{\rm NM}$ can be treated as a constant when synaptic events in the dendrites are modeled as independent, randomly-generated Poisson processes with the same frequency. In this model, the total number of synaptic inputs is set to 420 and the conductance of each synaptic current is $g_{\rm NM}=0.5$ nS.

It should be noted that both exogenous and endogenous EF are time-varying and heterogeneous in the brain. Studies on time-varying EF focus on the entrainment effect of EF on neuronal activities. In this study, we aimed to explore how EF modulates multi-timescale neuronal oscillations. At the single neuron level, a low-frequency EF can be treated as homogeneous and modeled as a uniform EF. Hence, we introduced a uniform EF in volts per meter (in units of V/m), aligned parallel to the somato-dendritic axis, in pyramidal cells by using the extracellular mechanism in NEURON.[31] Then we defined the orientation, including anodal and cathodal stimulation, based on the polarization profile induced in the neurons. During anodal stimulation, the positive electrode was positioned closer to the apical dendrites of cortical pyramidal cells, while during cathodal stimulation, the negative electrode was positioned closer to the apical dendrites.

2.2. A simplified neuronal model

In our previous study,[24] we found that the EF stimulation exhibits varying sensitivity depending on the number of dendritic branches generating NMDA spikes, suggesting that the number of dendritic branches involved in generating these spikes could influence the modulation effect of EF stimulation on dendritic oscillations. To investigate the modulation sensitivity of EF stimulation with varying numbers of dendritic branches generating NMDA and Ca^{2+} oscillations, we developed a simplified neuronal model consisting of one soma, one trunk, and five basal and apical dendrites (Fig. 2(a)). As described above, the soma, trunk, and basal dendrites are responsible for generating Na^{+} spikes, dendritic Ca^{2+} oscillations, and NMDA oscillations, respectively. Similar to the layer 5 pyramidal neuron, the membrane resistivity, axial resistivity, and membrane capacitance of the simplified model were set to 20 kΩ·cm^2, 530 Ω·cm, and 1.2 μF/cm^2, respectively. It should be noted that the simplified neuron lacks an axon, which results in increased concentration of somatic sodium ions to reproduce the action potential observed in the biophysical model. Additionally, the absence of a "hot zone" makes the apical dendrite require more calcium ions to generate calcium spikes. Hence, the active ionic channels in the model are distributed as follows:

Soma: $g_{\rm Na}=4000$ pS/μm^2, $g_{\rm K}=6000$ pS/μm^2. Basal dendrites: $g_{\rm L}=1$ pS/μm^2, $g_{\rm Ca}=9.75$ pS/μm^2, $g_{\rm KC}=100$ pS/μm^2, $g_{\rm KCa}=10$ pS/μm^2, $g_{\rm Kdr}=1000$ pS/μm^2. Trunk: $g_{\rm K}=600$ pS/μm^2, $g_{\rm L}=1$ pS/μm^2, $g_{\rm Ca}=6.5$ pS/μm^2, $g_{\rm KC}=80$ pS/μm^2, $g_{\rm KCa}=1$ pS/μm^2, $g_{\rm Kdr}=300$ pS/μm^2. Apical dendrite: $g_{\rm L}=1$ pS/μm^2, $g_{\rm Ca}=43$ pS/μm^2, $g_{\rm KC}=140$ pS/μm^2, $g_{\rm KCa}=100$ pS/μm^2, $g_{\rm Kdr}=2$ pS/μm^2.

The kinetics of NMDA synaptic inputs were described by Eq. (9), with a maximum conductance of 1.51 nS. A total of 125 synaptic inputs were uniformly distributed across the five basal dendrites, with a 6–μ m distance between adjacent synapses. The EF was simulated using the extracellular mechanism, with its orientation defined as described above. When the simplified neurons were subjected to cathodal stimulation, the apical dendrites were depolarized, while the soma and basal dendrites were hyperpolarized. In contrast, anodal stimulation caused hyperpolarization in the apical dendrites while simultaneously depolarizing both the basal dendrites and soma (Fig. 2(b)).

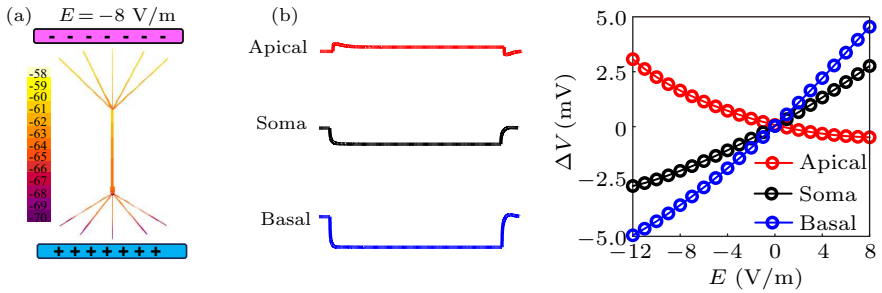


Fig. 2. A simplified neuronal model simulating multi-timescale neuronal oscillations. (a) False color map of membrane voltage at $E=-8$ V/m, (b) voltage traces recorded in the soma (black), apical (red), and basal (blue) dendrite at $E=-8$ V/m, and the membrane polarization ΔV in the soma (black circle), apical (red circle), and basal (blue circle) dendrite as a function of EF.

2.3. A three-compartment model of multi-timescale compound oscillation

As described above, there exist multi-timescale neuronal oscillations during epileptiform discharge, which include slow dendritic Ca^{2+} oscillation, fast dendritic NMDA oscillation and fastest somatic Na^{+} oscillation. However, the biophysical neuronal model involves a large number of parameters, making it challenging to analyze the dynamic mechanisms by which EF modulates these multi-timescale oscillations. Thus, we constructed a three-compartment model, which can characterize the input–output relationship of the layer 5 pyramidal neuron described above. As shown in Fig. 3(a), the model consists of an apical dendrite, a basal dendrite and a soma, which are responsible for generating dendritic Ca^{2+} and NMDA oscillations as well as somatic Na^{+} oscillations, respectively. The morphology of each compartment in the three-compartment model was defined as follows: the somatic compartment has the combined area of the biological soma and axon, the apical dendritic compartment area corresponds to the total area of all apical dendritic branches, and the basal dendritic compartment area corresponds to the total area of all basal dendritic branches. In this model, the somatic compartment was represented as a sphere, with its diameter equal to its length. The diameter of the apical dendrite compartment equals the average diameter of all apical dendrites of a layer 5 pyramidal neuron. And the diameter of the basal dendritic compartment was defined as the average diameter of all basal dendrites. Namely, the soma has an area (A_s) of 2461.09 μm^2 and a diameter of 15μm. Both the apical and basal dendritic compartments have a diameter of 6.5 μm, with the apical dendrite having an area (A_{ad}) of 35758.26 μm^2 and the basal dendrite having an area (A_{bd}) of 10070.68 μm^2, respectively. According to the method in Ref. [15], we set about half lengths of dendrites, *i.e.*, 1100 μm for the distance between the apical dendritic and somatic compartments, and 200 μm for the distance between the basal dendritic and somatic compartments, respectively. And the parameters of axial resistance and membrane capacitance were $R_a = 530$ Ω·cm and $C = 1.2$ μF/cm^2, respectively. The membrane resistance of the basal and apical dendrites was 20000 Ω·cm^2, and the somatic membrane resistance was 680 Ω·cm^2. Further, the apical dendritic compartment included I_{Ca}, I_{KC}, and I_{KAHP} in order to generate dendritic Ca^{2+} oscillations. The soma included I_K and I_{Na} to generate action potentials. And the basal dendritic compartment included I_{Kdr} and I_{NMDA} in order to generate dendritic NMDA oscillations. Therefore, under EF stimulation the transmembrane potential dynamics of the apical dendrite (V_{m_ad}), soma (V_{ms}), and basal dendrite (V_{m_bd}) of the three-compartment neuronal model can be described as follows:

$$\begin{aligned}
\frac{\mathrm{d}V_{m_ad}}{\mathrm{d}t} &= \frac{1}{C}\Bigg(-I_{Ca}-I_{KC}-I_{KHAP}-I_{Lad} \\
&\quad -\frac{g_{cs_ad}}{A_{ad}}\left(V_{m_ad}-V_{ms}+E\times L_{ad_s}\right)\Bigg), \\
\frac{\mathrm{d}V_{ms}}{\mathrm{d}t} &= \frac{1}{C}\Bigg(-I_{Ls}-I_{K}-I_{Na} \\
&\quad +\frac{g_{cs_ad}}{A_s}\left(V_{m_ad}-V_{ms}+E\times L_{ad_s}\right) \\
&\quad -\frac{g_{cs_bd}}{A_s}\left(V_{ms}-V_{m_bd}+E\times L_{bd_s}\right)\Bigg), \\
\frac{\mathrm{d}V_{m_bd}}{\mathrm{d}t} &= \frac{1}{C}\Bigg(-I_{Lbd}-I_{Kdr}-I_{NMDA} \\
&\quad +\frac{g_{cs_bd}}{A_{bd}}\left(V_{ms}-V_{m_bd}+E\times L_{bd_s}\right)\Bigg),
\end{aligned} \tag{10}$$

where $g_{cs_ad} = 5.692\times10^{-6}$ represents the coupling conductance between the somatic compartment and apical dendrite, and $g_{cs_bd} = 3.131\times10^{-5}$ represents the coupling conductance between the somatic compartment and basal dendrite; E represents the EF stimulation. And the ionic current in each compartment was depicted as follows:

$$\begin{aligned}
I_{Ca} &= g_{Ca}m_{Ca}^2h_{Ca}\left(V_{m_ad}-E_{Ca}\right), \\
I_{KC} &= g_{KC}c\chi\left(Ca\right)\left(V_{m_ad}-E_{K}\right), \\
I_{KHAP} &= g_{KHAP}q\left(V_{m_ad}-E_{K}\right), \\
I_{Lad} &= g_{Lad}\left(V_{m_ad}-E_{L}\right), \\
I_{K} &= g_{K}w\left(V_{ms}-E_{K}\right), \\
I_{Na} &= g_{Na}m_{\infty}\left(V_{ms}\right)\left(V_{ms}-E_{Na}\right), \\
I_{Ls} &= g_{Ls}\left(V_{ms}-E_{L}\right), \\
I_{Kdr} &= g_{Kdr}n^4\left(V_{m_bd}-E_{K}\right), \\
I_{NMDA} &= g_{NM}B\left(V_{m_bd}\right)\left(V_{m_bd}-E_{NMDA}\right), \\
I_{Lbd} &= g_{Lbd}\left(V_{m_bd}-E_{L}\right),
\end{aligned} \tag{11}$$

where $g_{Ca} = 1.4$ mS/cm^2, $g_{KC} = 0.015$ mS/cm^2, $g_{KAHP} = 0.05$ mS/cm^2, $g_{Lad} = 0.05$ mS/cm^2, $g_K = 32$ mS/cm^2, $g_{Na} = 9$ mS/cm^2, $g_{Ls} = 1.47$ mS/cm^2, $g_{Kdr} = 30$ mS/cm^2, $g_{NM} = 1.7$ mS/cm^2, $g_{Lbd} = 0.05$ mS/cm^2. And the reversal potentials were $E_{Ca} = 20$ mV, $E_K = -80$ mV, $E_{Na} = 50$ mV, $E_L = -70$ mV, and $E_{NMDA} = 0$ mV. The dynamics of I_{Ca}, I_{Kdr}, I_{KC}, and I_{KAHP} as well as the calcium concentration were the same as the descriptions in Subsection 2.1. And the w was the activation variable for I_K, which is governed by the following equation:

$$\frac{\mathrm{d}w}{\mathrm{d}t} = \varphi\frac{\left(w_{\infty}\left(V_{ms}\right)-w\right)}{\tau_w}, \tag{12}$$

where $w_{\infty}\left(V_{ms}\right)$ and τ_w represent the steady-state value and time constant for w. And they can be described as follows:

$$\begin{cases} w_{\infty} = 0.5\left(1+\tanh\left(V_{ms}/10\right)\right), \\ \tau_w = 1/\cosh\left(V_{ms}/20\right). \end{cases} \tag{13}$$

And the steady-state value $m_{\infty}\left(V_{ms}\right)$ for I_{Na} can be described by

$$m_{\infty} = 0.5\left(1+\tanh\left(\left(V_{ms}+1.2\right)/18\right)\right). \tag{14}$$

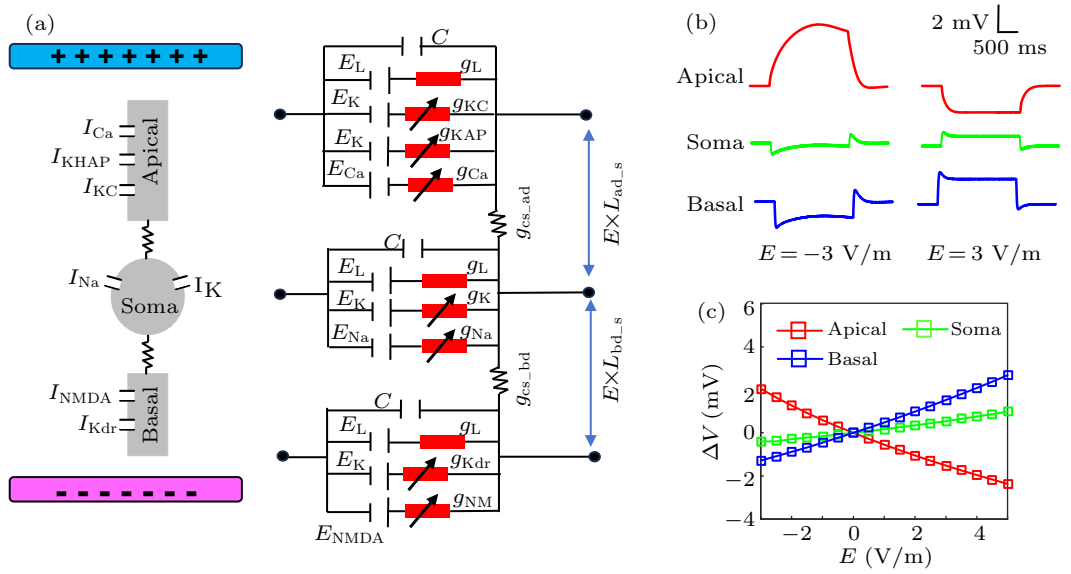


Fig. 3. The schematic diagram of three-compartment model and its polarization response to EF stimulation. (a) Three-compartment model of layer 5 pyramidal neuron, including soma, apical, and basal dendritic compartments; (b) voltage traces recorded in the soma (green), apical (red) and basal (blue) dendrite at $E = -3$ V/m and $E = 3$ V/m; (c) the membrane polarization ΔV in the soma (green square), apical (red square), and basal (blue square) dendrites as a function of EF.

When the three-compartment model was stimulated with EF, the apical dendrite of the three-compartment model was depolarized in the case of cathodal stimulation while the soma and basal dendrites were hyperpolarized (Figs. 3(b) and 3(c)). In contrast, the apical dendrite was hyperpolarized under anodal stimulation while both the basal dendrite and soma were depolarized simultaneously (Figs. 3(b) and 3(c)).

2.4. Dendritic oscillation sensitivity to EF

It is found that dendritic integration across multiple dendritic branches is nonlinear,[30] for example, the dendritic integration of layer 2/3 pyramidal neurons is superlinear when computed across multiple dendritic branches, while that of layer 5 pyramidal neurons is linear or sublinear. To characterize the nonlinear dendritic integration, Tran–Van–Minh *et al.*[11] compared the observed excitatory postsynaptic potentials (EPSPs) resulting from the simultaneous activation of the same synaptic inputs with the arithmetic sum of individual EPSPs (also referred to as the expected EPSPs). Similarly, we used the relationship between the expected axial current and the observed axial current across multiple dendritic branches to characterize the nonlinear effects of the EF modulation. We defined the average EF intensity required to trigger the dendritic NMDA spike or Ca^{2+} spike of a single dendritic branch as the modulatory sensitivity of EF (ESS):

$$\mathrm{ESS} = E_{\mathrm{thresh}}/n_{\mathrm{bran}}. \tag{15}$$

To observe the nonlinear dendritic integration as different numbers of dendritic branches generate dendritic NMDA spikes with increasing EF intensity, we selected 7 dendritic branches for the layer 5 pyramidal neuron, each containing 23 NMDA synapses. For the simplified cable model, 5 basal dendrites were chosen with 25 NMDA synapses uniformly distributed across each branch, positioned 100 μm away from the soma. The distance between two adjacent synapses was 6 μm. Then the axial current from basal dendrites to the soma was recorded. In this case, $g_{\mathrm{Ca}} = 0$. To examine the nonlinear dendritic integration caused by dendritic Ca^{2+} spikes, we selected 3 dendritic branches from the hot zone for the pyramidal neuron. For the simplified neuronal model, 5 apical dendrites were chosen. In this case, $g_{\mathrm{NM}} = 0$. The axial current from the trunk to the soma was subsequently recorded.

3. Results

3.1. The multi-timescale compound oscillation induced by EF stimulation

It has been shown that there exist multi-timescale neuronal oscillations during epileptiform discharges, including slow and fast dendritic oscillations as well as fastest somatic Na^{+} oscillations. Chiang *et al.*[16] found that the slow oscillation depends on dendritic Ca^{2+} spikes while the fast oscillation relies on dendritic NMDA spikes. Furthermore, they demonstrated that the propagation of dendritic oscillations is influenced by EF stimulation. These findings suggest an interaction among dendritic Ca^{2+} spikes, NMDA spikes, and somatic action potentials when neurons are subjected to EF stimulation. To investigate the modulatory effect, we first built a pyramidal neuron with complex morphology to explore whether cathodal EF stimulation or anodal EF stimulation can induce multi-timescale oscillation interactions.

As shown in Fig. 4, in the case of $E = 16$ V/m, the EF-induced depolarization at basal dendrites leads to a dendritic

NMDA spike, while the hyperpolarization at the apical dendrite prevents the generation of dendritic Ca^{2+} oscillations by reducing excitability (Fig. 4(a)). In contrast, under cathodal stimulation with $E = -3$ V/m, the depolarization of apical dendrites increases dendritic excitability, but the effect is too small to induce dendritic Ca^{2+} oscillations (Fig. 4(b)). The hyperpolarization of basal dendrites prevents the generation of a dendritic NMDA spike. At $E = -6$ V/m, the layer 5 pyramidal neuron generates a multi-timescale compound oscillation (Fig. 4(c)), including the slowest dendritic Ca^{2+} oscillation with a timescale of 522 ms, a faster dendritic NMDA oscillation with a timescale of 100 ms, and the fastest somatic Na^{+} oscillation with a timescale of 5 ms. Decades of experimental and modeling studies[12,28] have shown that the timescale of a dendritic Ca^{2+} spike is on the order of several hundred milliseconds, the timescale of dendritic NMDA discharges is approximately 100 milliseconds, and the timescale of somatic Na^{+} spikes is on the order of a few milliseconds. Our results are consistent with these experimental and modeling findings.

Further, our results show that apical dendritic depolarization triggers dendritic Ca^{2+} oscillations at first (Fig. 4(d)). Subsequently, the current flowing into the basal dendrites enhances dendritic excitability, leading to the generation of dendritic NMDA oscillations (Fig. 4(d)). Together, the dendritic NMDA and Ca^{2+} oscillations increase somatic excitability, which in turn leads to the generation of action potentials (Fig. 4(d)). This suggests that a dendritic Ca^{2+} spike serves as the source for the generation of dendritic NMDA oscillations. To test this hypothesis, we examined the EF stimulation thresholds required to generate dendritic Ca^{2+} oscillations, NMDA oscillations, and somatic Na^{+} spikes. As shown in Fig. 4(d), we found that dendritic Ca^{2+} oscillations require the smallest EF intensity, while dendritic NMDA spikes need a larger EF intensity, and the initiation of action potentials requires the largest EF intensity, regardless of the EF orientation. These findings provide an explanation for the experimental observation[16] that the propagation onset of dendritic NMDA oscillations depends on the preceding dendritic Ca^{2+} oscillations. Together, these results suggest that this model can be used to explore how EF regulates multi-timescale compound oscillations in neurons.

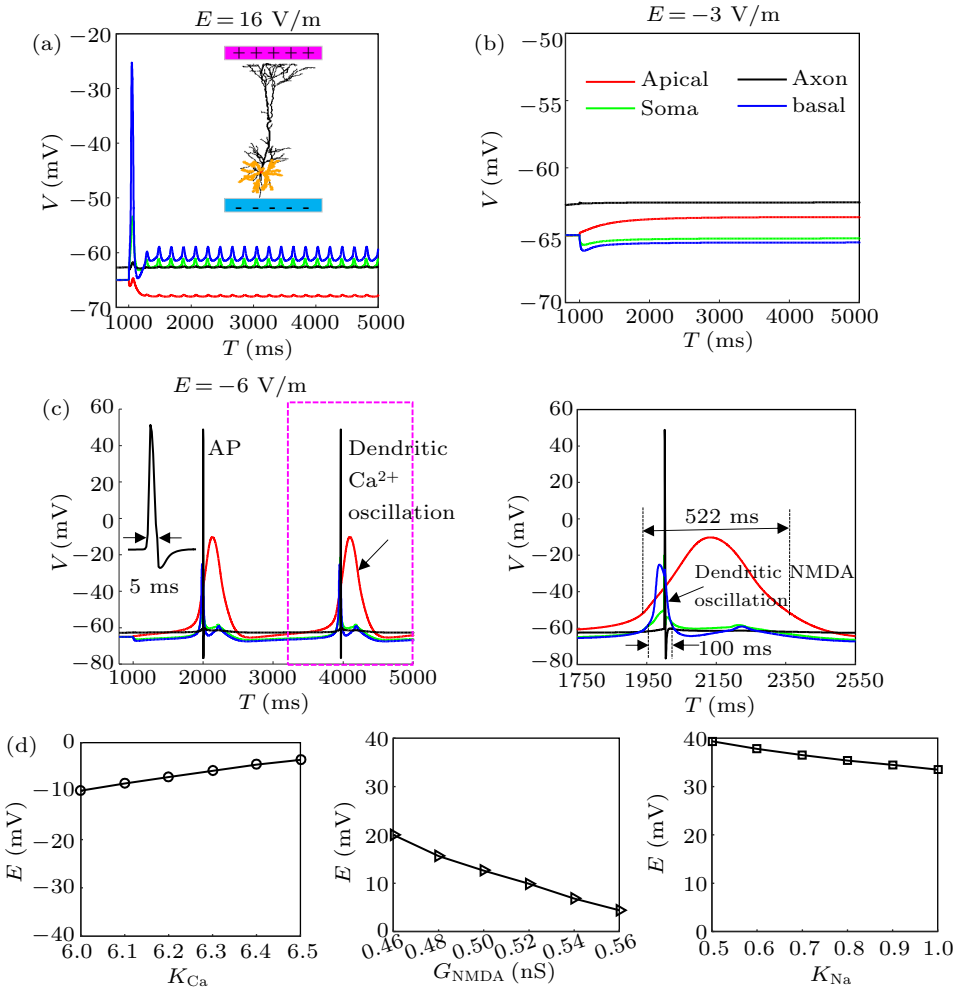


Fig. 4. A layer 5 pyramidal neuron depicting EF-regulated multi-timescale neuronal oscillations: (a)–(c) the varying membrane potential of soma, axon, apical, and basal dendrites with time when $E = 16$ V/m, -3 V/m, and -6 V/m, respectively; (d) the EF stimulation threshold for triggering dendritic Ca^{2+} (left), NMDA (middle) oscillations as well as somatic action potential (right) when the calcium, NMDA, and sodium conductance changes. K_{Ca} and K_{Na} represent the scaling factors for g_{Ca} and g_{Na}, respectively.

3.2. The modulation effect of EF on multi-timescale compound oscillation

Previous studies [21,32,33] have pointed out that EF stimulation could modulate neuronal spike patterns and timing, which are determined by the intrinsic dynamics of the neuron. To investigate the modulatory effect of EF on multi-timescale compound oscillations, we examined the variation in the mean interspike interval (ISI) of dendritic Ca^{2+} oscillations and the timing of the first dendritic Ca^{2+} spike for different values of g_{NM}.

When $g_{NM} = 0.5$ nS, increased dendritic depolarization induces more dendritic Ca^{2+} spikes, which leads to a greater axial current flowing into the soma, thereby resulting in an increased number of somatic action potentials (Fig. 5(a)). However, stronger cathodal EF stimulation causes more pronounced somatic hyperpolarization, which cannot be compensated by the increasing axial current, resulting in a decrease in the number of APs as the cathodal EF intensity increases (Fig. 5(a)). When $g_{NM} = 0.6$ nS, we observed a similar modulatory influence of the EF on the multi-timescale compound oscillations (Fig. 5(b)). Differently, an increase in g_{NM} makes the basal dendrites generate two dendritic NMDA spikes within a single dendritic Ca^{2+} spike (Fig. 5(b)), which leads to somatic burst discharge. Furthermore, our results show that increasing EF intensity reduces both the mean ISI and the spike timing of the first dendritic Ca^{2+} spike (Fig. 5(c) and Fig. 5(d)). The increase in g_{NM} results in a longer mean ISI and a delayed spike timing for the first dendritic Ca^{2+} spike (Fig. 5(c) and Fig. 5(d)). These results suggest that the intrinsic neuronal properties play a crucial role in determining its compound oscillation in response to EF stimulation.

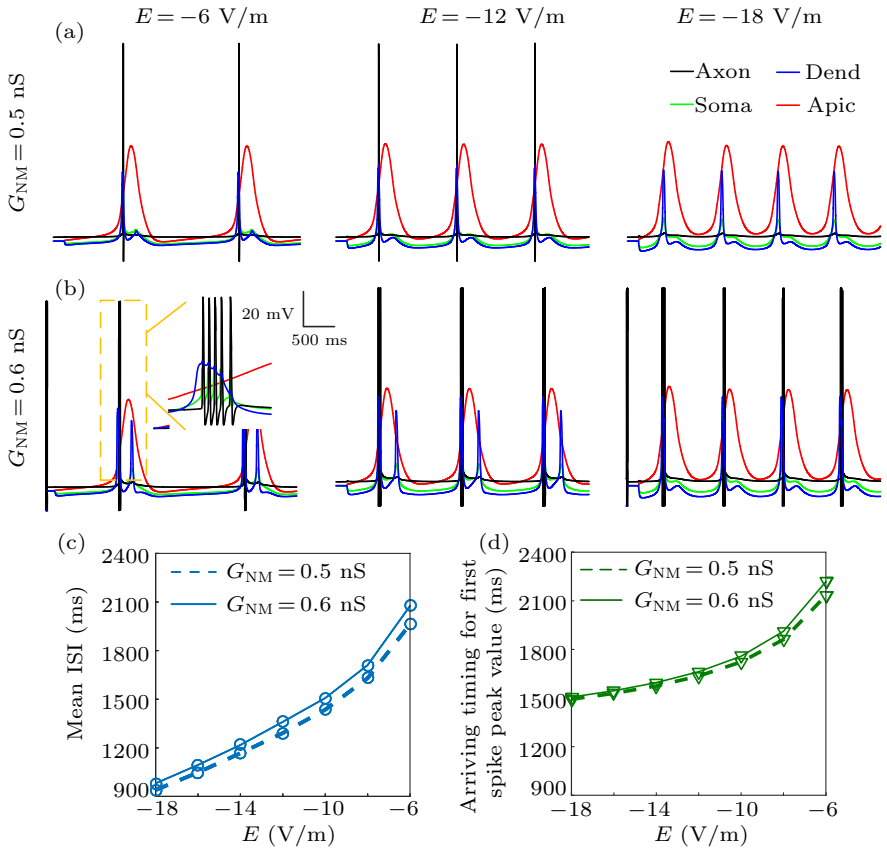


Fig. 5. The modulation influence of EF on multi-timescale neuronal oscillations for different NMDA conductances: (a)–(b) varying membrane potential of soma (green), axon (black), apical (red), and basal (blue) dendrites with time when $g_{NM} = 0.5$ nS and $g_{NM} = 0.6$ nS, respectively; (c)–(d) the mean ISI and the spike timing of the first dendritic Ca^{2+} spike as a function of EF intensity when $g_{NM} = 0.5$ nS and $g_{NM} = 0.6$ nS, respectively.

3.3. A three-compartment model reproducing multi-timescale dendritic oscillations

The above results obtained from the realistic neuronal model demonstrate the EF modulatory effect on multi-timescale compound oscillations. However, the dynamic mechanism by which EF modulates these oscillations remains unclear. As is well known, the layer 5 pyramidal neuron is challenging to analyze due to its complex dendritic morphology. Our previous studies[32,33] have shown that the two-compartment model, using a coupling coefficient g_c to depict the EF influence on dendrites and soma, can be effectively used to study the dynamic variation of a neuron when it is subjected to EF stimulation. Building on this work, we developed a three-compartment model (Fig. 3) to explore how EF modulates the multi-timescale neuronal oscillations.

First, we explored the modulation effect of EF when

$E = 12$ V/m. It is shown that the dendritic depolarization at basal dendrites triggers dendritic NMDA spikes, which also increase the somatic membrane potential. At the same time, the generation of dendritic Ca^{2+} spikes is difficult, since the EF-induced hyperpolarization at apical dendrites decreases excitability (Fig. 6). This suggests that the anodal stimulation fails to trigger multi-timescale neuronal oscillations. Then, we changed EF stimulation to cathodal stimulation. At $E = -6$ V/m, no dendritic spike is observed. Only at $E = -7$ V/m does the pronounced dendritic depolarization at apical dendrites lead to the generation of dendritic Ca^{2+} oscillations, which in turn trigger dendritic NMDA oscillations. Despite this, no somatic Na^{+} is observed at this stage. Only when $E = -9$ V/m, the interaction among dendritic NMDA oscillations, Ca^{2+} oscillations, and somatic Na^{+} discharge appears. Compared with the layer 5 pyramidal neuron, the stimulation threshold in the three-compartment model is higher, suggesting that the three-compartment model does not fully capture the input–output relationship of layer 5 pyramidal neurons.

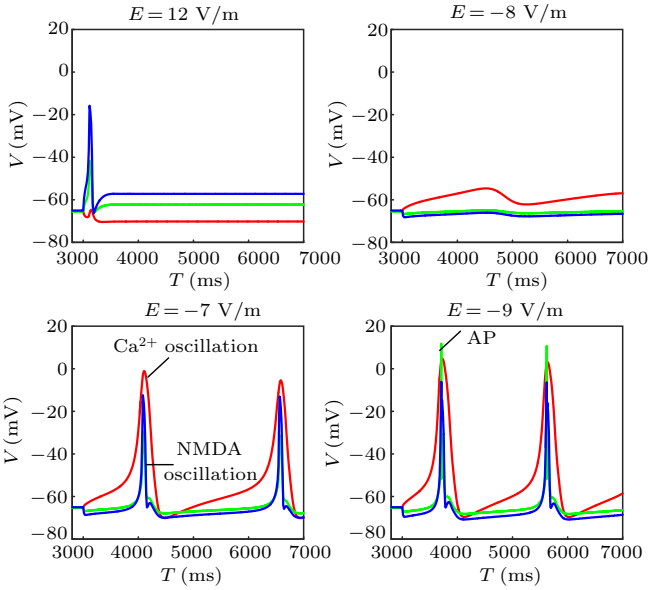


Fig. 6. The input–output relationship of three-compartment model for different EF intensities. These red, blue, and green lines represent the membrane potential of dendritic Ca^{2+} and NMDA oscillations as well as somatic Na^{+} spike.

3.4. Modulation sensitivity of EF for dendritic oscillations

These results above indicate that the EF modulation sensitivity of the three-compartment model is lower than that of the layer 5 pyramidal neuron. Our previous study[24] demonstrated that EF modulation sensitivity increases with the number of dendritic branches generating dendritic NMDA spikes. Based on this, we hypothesize that the coupling coefficient of the EF should be greater than the axial conductance. To test this hypothesis, we first quantified the EF modulation sensitivity, as a different number of dendritic branches generate dendritic oscillations, as shown in Fig. 7.

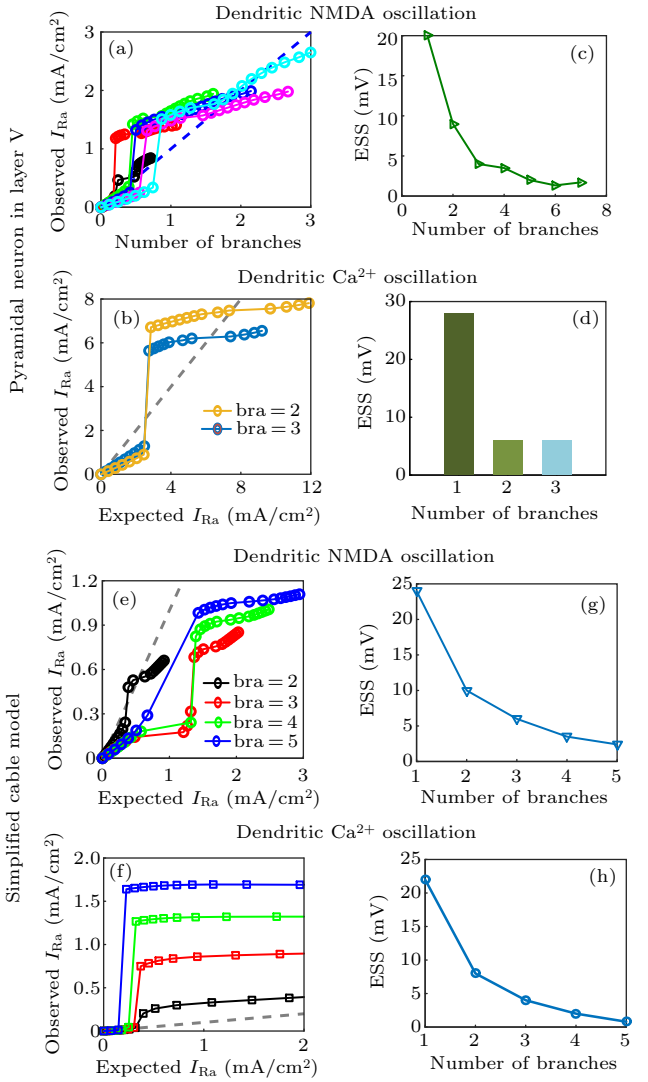


Fig. 7. The modulation sensitivity of EF to different oscillations: (a) and (c) The dendritic integration relationship and ESS when multiple dendritic branches of the realistic pyramidal neuron generate dendritic NMDA spike, respectively; (b) and (d) similar to panels (a) and (c), but for dendritic Ca^{2+} spike; (e) and (g) the dendritic integration relationship and ESS when multiple dendritic branches of the simple cable neuron generate dendritic NMDA spike, respectively; (f) and (h) similar to panels (e) and (f), but for dendritic Ca^{2+} spike.

We observed that the EF stimulation threshold decreases as the number of dendritic branches generating NMDA (Fig. 7(a)) or Ca^{2+} spikes (Fig. 7(b)) increases. By calculating the ESS, we found that EF modulation sensitivity increases with the increasing dendritic branches, due to interactions between dendritic spikes across multiple dendrites (Figs. 7(c) and 7(d)). Additionally, we found that EF stimulation modulates dendritic NMDA and Ca^{2+} oscillations in a nonlinear manner. Using a simplified cable model, we further demonstrated that the nonlinear modulation effect of the EF is closely related to the number of dendritic branches (Figs. 7(e) and 7(f)). Our results indicate that the modulation sensitivity of EF increases with the number of dendritic branches, and the EF regulates dendritic oscillations across multiple branches in a nonlinear way (Figs. 7(g) and 7(h)).

3.5. A modified three-chamber model reproducing multi-timescale compound oscillation

The above results suggest that a higher coupling coefficient is required to accurately characterize the nonlinear EF modulation sensitivity. Given the differing EF modulation sensitivities for dendritic Ca and NMDA oscillation, we introduced Coff to describe the contribution of the EF-regulated dendritic Ca oscillation to the soma, and used Coff to represent the influence of the EF-regulated dendritic NMDA spike on the soma. By fitting the input–output relationship between the layer 5 pyramidal neuron and the three-compartment model, we obtained a modified three-compartment model depicted as follows:

$$C\frac{\mathrm{d}\boldsymbol{X}}{\mathrm{d}t}=\boldsymbol{F}(\boldsymbol{X},U)=[F_1,F_2,F_3,F_4,F_5,F_6,F_7,F_8,F_9,F_{10}]^{\mathrm{T}},\quad(16)$$

where

$$\begin{aligned}
F_1 &= \frac{1}{C}\Big(-g_{\mathrm{Ca}}m_{\mathrm{Ca}}^2h_{\mathrm{Ca}}(V_{\mathrm{m_ad}}-E_{\mathrm{Ca}})-g_{\mathrm{KC}}c\chi(Ca)\\
&\quad\times(V_{\mathrm{m_ad}}-E_{\mathrm{K}})-\frac{g_{\mathrm{cs_ad}}}{A_{\mathrm{ad}}}(V_{\mathrm{m_ad}}-V_{\mathrm{ms}})\\
&\quad-g_{\mathrm{KHAP}}q(V_{\mathrm{m_ad}}-E_{\mathrm{K}})-g_{\mathrm{Lad}}(V_{\mathrm{m_ad}}-E_{\mathrm{L}})\\
&\quad+I_{\mathrm{bias_ad}}-\frac{\mathrm{Coff_{ad}}\times L_{\mathrm{ad_}s}\times E}{A_{\mathrm{ad}}}\Big),\\
F_2 &= \frac{1}{C}\Big(-g_{\mathrm{K}}w(V_{\mathrm{ms}}-E_{\mathrm{K}})-g_{\mathrm{Na}}m_{\infty}(V_{\mathrm{ms}})\\
&\quad\times(V_{\mathrm{ms}}-E_{\mathrm{Na}})-\frac{g_{\mathrm{cs_bd}}}{A_s}(V_{\mathrm{ms}}-V_{\mathrm{m_bd}})\\
&\quad+\frac{g_{\mathrm{cs_ad}}}{A_s}(V_{\mathrm{m_ad}}-V_{\mathrm{ms}})-g_{\mathrm{Ls}}(V_{\mathrm{ms}}-E_{\mathrm{L}})+I_{\mathrm{bias_s}}\\
&\quad+\frac{\mathrm{Coff_{ad}}\times L_{\mathrm{ad_}s}\times E}{A_s}-\frac{\mathrm{Coff_{bd}}\times L_{\mathrm{bd_s}}\times E}{A_s}\Big),\\
F_3 &= \frac{1}{C}\Big(-g_{\mathrm{Lbd}}(V_{\mathrm{m_bd}}-E_{\mathrm{L}})-g_{\mathrm{Kdr}}n^4(V_{\mathrm{m_bd}}-E_{\mathrm{K}})\\
&\quad+\frac{g_{\mathrm{cs_bd}}}{A_s}(V_{\mathrm{ms}}-V_{\mathrm{m_bd}})-\bar{g}_{\mathrm{NMDA}}B(V_{\mathrm{m_bd}})\\
&\quad\times(V_{\mathrm{m_bd}}-E_{\mathrm{NMDA}})+I_{\mathrm{bias_bd}}+\frac{\mathrm{Coff_{bd}}\times L_{\mathrm{bd_s}}\times E}{A_{\mathrm{bd}}}\Big),\\
F_4 &= (m_{\mathrm{Ca}\infty}(V_{\mathrm{m_ad}})-m_{\mathrm{Ca}})/\tau_{\mathrm{mCa}},\\
F_5 &= (h_{\mathrm{Ca}\infty}(V_{\mathrm{m_ad}})-h_{\mathrm{Ca}})/\tau_{\mathrm{hCa}},\\
F_6 &= (c_{\infty}(V_{\mathrm{m_ad}})-c)/\tau_c,\\
F_7 &= \left(q_{\infty}\left(\left[\mathrm{Ca}^{2+}\right]_i\right)-q\right)/\tau_{\mathrm{q}},\\
F_8 &= -vI_{\mathrm{Ca}}-\left[\mathrm{Ca}^{2+}\right]_i/\tau_{[\mathrm{Ca}]},\\
F_9 &= \varphi\frac{(w_{\infty}(V_{\mathrm{ms}})-w)}{\tau_w},\\
F_{10} &= (n_{\infty}(V_{\mathrm{m_bd}})-n)/\tau_n.
\end{aligned}\quad(17)$$

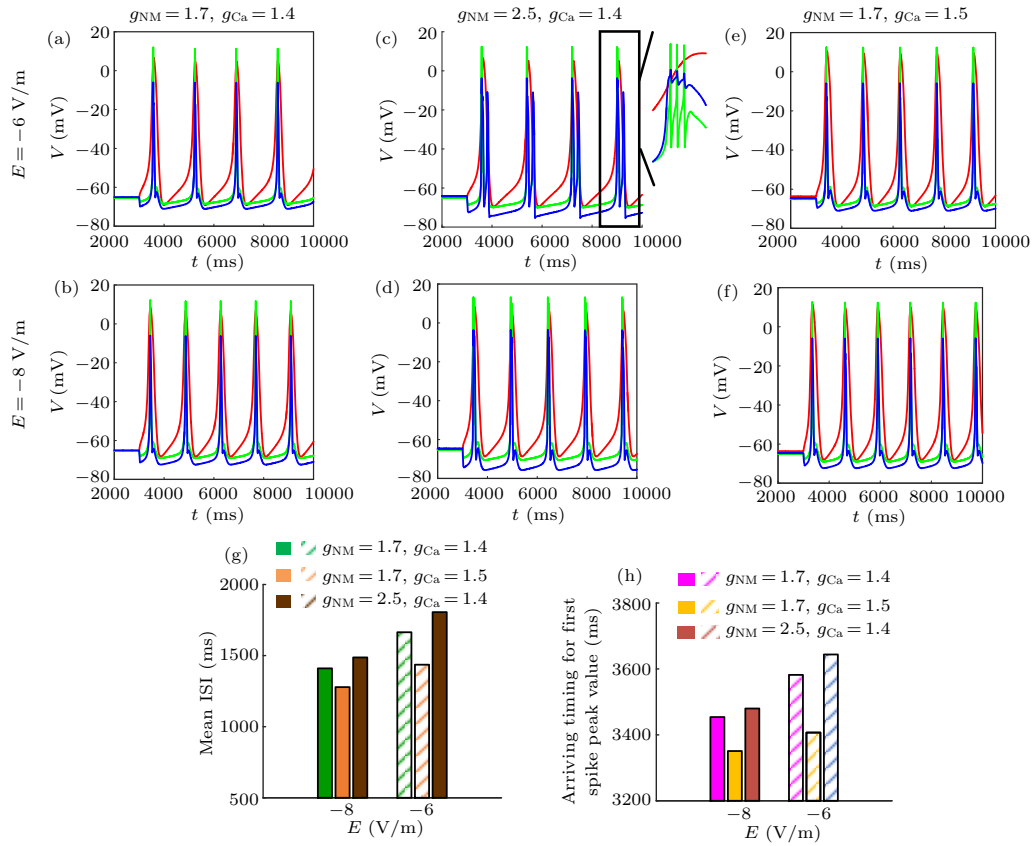


Fig. 8. The modulatory effect of EF on multi-timescale oscillations of the modified three-chamber model: (a) and (b) voltage waveforms of soma (green), apical dendrite (red), and basal dendrite (blue) at $E=-6$ V/m or -8 V/m, respectively, when $g_{\mathrm{NM}}=1.7$ mS/cm^2 and $g_{\mathrm{Ca}}=1.4$ mS/cm^2; (c) and (d) similar to panels (a) and (b), but for $g_{\mathrm{NM}}=1.7$ mS/cm^2 and $g_{\mathrm{Ca}}=1.5$ mS/cm^2; (e) and (f) similar to panels (a) and (b), but for $g_{\mathrm{NM}}=2.5$ mS/cm^2 and $g_{\mathrm{Ca}}=1.4$ mS/cm^2; (g) and (h) the mean ISI and the spike timing of first dendritic Ca^{2+} spike when $g_{\mathrm{NM}}=1.7$ mS/cm^2 and $g_{\mathrm{NM}}=2.5$ mS/cm^2, respectively.

Here $\text{Coff}_{\text{ad}} = 1.029 \times 10^{-5}$ and $\text{Coff}_{\text{bd}} = 4.69 \times 10^{-5}$. Then, we performed numerical simulation using Eq. (15), and found that when $g_{\text{NM}} = 1.7$ mS/cm^2, the modified three-compartment neuronal model begins to generate multi-timescale compound neuronal oscillations for $E = -6$ V/m (Fig. 8(a)). When $E = -8$ V/m, the number of dendritic Ca^{2+} and NMDA spike as well as the somatic Na^+ discharge increases due to more significant dendritic depolarization in the apical dendrites (Fig. 8(b)). As we increased g_{NM} to 2.5 mS/cm^2, the basal dendritic compartment generates two dendritic NMDA spike for each dendritic Ca^{2+} spike and the soma exhibited burst spike within a dendritic NMDA spike (Figs. 8(c) and 8(d))). As g_{Ca} increased from 1.4 mS/cm^2 to 1.5 mS/cm^2, the neuron still generates tonic spike (Figs. 8(e) and 8(f)). The increase in g_{NM} resulted in increasing mean ISI and arrival time of the peak value of the first dendritic Ca^{2+} spike (Figs. 8(g) and 8(h)) while the increasing g_{Ca} leads to a decreasing mean ISI and arrival time of the peak value of the first dendritic Ca^{2+} spike (Figs. 8(g) and 8(h)). By calculating the variation of mean ISI for unit g_{NM} and g_{Ca}, we found that the system is more sensitive to the variation of g_{Ca} (g_{NM}: 390 ms/mS/cm^2; g_{Ca}: 872.5 ms/ mS/cm^2), which indicates the important role of dendritic Ca^{2+} oscillation in triggering multi-timescale neural oscillations. These results are consistent with the behavior observed in layer 5 pyramidal neurons, suggesting that the modified three-compartment model successfully reproduced the input–output relationship of layer 5 pyramidal neurons under EF stimulation. Therefore, this model can be used to explore the dynamic mechanisms by which the EF modulates multi-timescale compound neuronal oscillations.

3.6. The dynamic mechanism of multi-timescale oscillation interaction under EF stimulation

Acting as a useful mathematical analysis tool, the singular perturbation method[34] is often used to separate subsystems with distinct timescales, which aids in analyzing complex multiscale dynamics. In the case of the modified three-chamber model, three types of dynamics with different timescales coexisted in the state equation Eq. (16), including the slowest dendritic Ca^{2+} spike timescale, a faster dendritic NMDA spike timescale, and the fastest somatic Na^+ discharge timescale. This multiscale nature complicates the analysis of the dynamic mechanisms underlying EF modulation. To address this challenge, we first reduced the system's dimensionality based on the time constants and then applied the singular perturbation method to decompose the neuronal system into three subsystems: a slow subsystem representing the apical dendritic dynamics, a faster subsystem describing basal dendritic dynamics, and the fastest subsystem characterizing the somatic action potential generation. In this case, the bifurcations of the three subsystems are responsible for the generation of dendritic Ca^{2+} oscillation, dendritic NMDA oscillation, and somatic Na^+ spike, respectively. The detailed derivation steps for key bifurcation identifications are provided in the Supporting Information. We subsequently performed dynamic analysis through numerical simulations, as shown in Fig. 9.

We found that anodal stimulation, which induces dendritic hyperpolarization, stabilizes the equilibrium point of the slowest subsystem, thereby maintaining the apical dendrite in a quiescent state (Fig. 9(a)). In this scenario, EF-induced depolarization improves the excitability of the soma and basal dendrites. Thus, the equilibrium points of the faster subsystem and the fastest subsystem gradually lose their stability and both undergo subcritical Andronov–Hopf bifurcations, leading to the generation of dendritic NMDA oscillation and somatic Na^+ oscillation, respectively. Our analysis revealed that the faster subsystem requires a smaller EF intensity to initiate dendritic NMDA oscillations compared to the fastest subsystem, which needs a higher EF intensity to trigger somatic Na^+ oscillations (Figs. 9(d) and 9(h)). These results indicate that anodal stimulation cannot cause the coexistence of multi-timescale compound neuronal oscillations.

Then we investigate the influence of cathodal stimulation. As described above, cathodal stimulation induces depolarization in the apical dendrites while causing hyperpolarization at the soma and basal dendrites. In this case, weak dendritic depolarization stabilizes the slowest subsystem's equilibrium point, and weak hyperpolarization at the soma and basal dendrites also stabilizes the faster and fastest subsystem's equilibrium points. Until $E = -0.8$ V/m, dendritic depolarization drives the slowest subsystem to experience a saddle-node on invariant circle (SNIC) bifurcation (Fig. 9(a)). This bifurcation causes the equilibrium point to transition from a stable state to an unstable state, making the onset of dendritic Ca^{2+} oscillations. The continuous f–E curve further supports this mechanism, indicating that dendritic Ca^{2+} oscillations emerge through an SNIC bifurcation (Fig. 9(b)). The generation of dendritic Ca^{2+} oscillations leads to increased current flow into the soma and basal dendrites, which compensates for the EF-induced hyperpolarization. Thus, the equilibrium point of the faster subsystem undergoes a subcritical Andronov–Hopf bifurcation and becomes an unstable equilibrium point as the membrane potential of apical dendrites increases (Fig. 9(c)). Consequently, dendritic NMDA oscillations are generated. The combination of dendritic NMDA and Ca^{2+} oscillations flowing into the soma improves its excitability. Hence, the fastest subsystem's equilibrium point undergoes a subcritical Andronov–Hopf bifurcation, triggering action potentials as the membrane potential of basal dendrites increases (Fig. 9(e)).

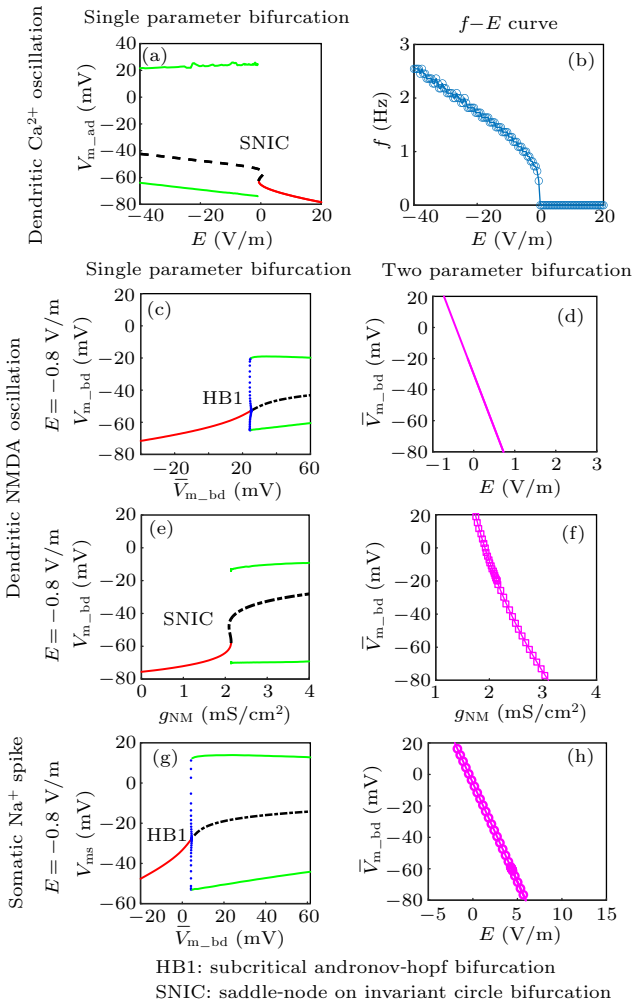


Fig. 9. The bifurcation diagram of the neuron to extracellular electric fields when the multi timescale oscillation generates: (a) single parameter bifurcation diagram when dendritic Ca^{2+} oscillation generates. The vertical axis shows the membrane potential of apical dendrites V_{m_ad} at the fixed point and at max/min of limit cycle as parameter E increases; (b) the average frequency of dendritic Ca^{2+} oscillation and extracellular EF curve (f–E) of the modified three-compartment neuron; (c) and (e) single parameter bifurcation when dendritic NMDA oscillation generates at $E = -0.8$ V/m. The vertical axis shows the membrane potential of basal dendrites V_{m_bd} at the fixed point and at max/min of limit cycle as parameter $\bar{V}_{m_ad}$ or gNM increases; (d) and (f) two parameter bifurcation when dendritic NMDA oscillation generates; (g) single parameter bifurcation diagram when somatic Na^+ spike generates. The vertical axis shows the somatic membrane potential V_{ms} at the fixed point and at max/min of limit cycle as parameter $\bar{V}_{m_bd}$ increases; (h) two parameter bifurcation when somatic Na^+ spike generates. (Stable steady state: red solid line; unstable steady state: black dotted line; stable limit cycle: green solid line; unstable limit cycle: blue dotted line). "HB1" refers to subcritical Andronov–Hopf bifurcation. "SNIC" refers to saddle-node on invariant circle bifurcation.

Additionally, we investigate the dynamic mechanism by which varying g_{NM} triggers dendritic NMDA oscillations under EF stimulation and find that in the case of constant cathodal stimulation and apical dendritic membrane potential ($\bar{V}_{m_ad}$), increasing g_{NM} causes the faster subsystem to experience an SNIC bifurcation to generate dendritic NMDA oscillations, following a supercritical Andronov–Hopf bifurcation to disappear (Fig. 9(e)). Observing the two-parameter bifurcation analysis between $\bar{V}_{m_ad}$ and g_{NM} (Fig. 9(f)), we find that a larger g_{NM} improves the basal dendrites' excitability to require a smaller $\bar{V}_{m_ad}$ to generate a dendritic NMDA spike. These results suggest that cathodal stimulation can cause the coexistence of multi-timescale compound neuronal oscillations, beginning with dendritic Ca^{2+} oscillation, followed by dendritic NMDA oscillations and finally somatic Na^+ spikes. The intrinsic properties, such as the conductance of NMDA synapses, play a crucial role in determining the EF modulation effect (Figs. 8 and 9(e)).

4. Conclusion and discussion

In this study, we built a biophysical pyramidal neuron model with complex morphology, capable of reproducing multi-timescale neuronal compound oscillations that resemble epileptiform discharges. Using this model, we investigated how an EF regulates these oscillations and examined the influence of ionic conductance on the EF modulation effects. Additionally, we explored the EF regulation sensitivity when multiple dendrites generate NMDA spikes or Ca^{2+} spikes, and observed that the EF modulation effect is nonlinear. Based on these findings, we proposed a minimal three-chamber model to describe the Ca–NMDA–Na compound oscillations under EF stimulation. This model allows us to analyze the dynamic mechanisms by which an EF modulates these interactions.

Experimental studies[14,16,20,35] have highlighted that the generation of epileptiform discharges depends on multi-timescale dendritic oscillations, which include the NMDA oscillation with a time constant around 100 milliseconds and a calcium oscillation with a time constant of several hundred milliseconds. Further, it is pointed out that in the absence of synaptic coupling, the propagation speeds of these oscillations depend on the EF intensity and direction.[35] To investigate the mechanisms underlying the coexistence of multi-timescale neuronal oscillations during epileptiform discharges, we built a pyramidal neuron model with complex dendritic morphology and found that dendritic depolarization induced by cathodal stimulation first activates dendritic Ca^{2+} channels, initiating dendritic Ca^{2+} oscillations with a time constant greater than 500 ms. These oscillations act as the source that triggers dendritic NMDA oscillations with a time constant of 100 ms. Subsequently, the interaction between dendritic Ca^{2+} spikes and NMDA spikes induces somatic Na^+ discharge with a time constant of 5 ms. This phenomenon aligns with experimental observations from Durand's research group,[20] supporting the validity of the pyramidal neuron model. Our findings illuminate the biophysical mechanisms that govern the interaction between fast and slow components of epileptiform waves under EF stimulation. Moreover, they suggest that anodal stimulation may suppress the generation of multi-timescale epileptiform oscillations, providing theoretical insights into the use of electromagnetic stimulation for epilepsy treatment.

Decades of experimental and modeling studies[32,36] have shown that neuronal intrinsic properties, such as dendritic morphologies and ionic dynamics, play important roles in EF-regulated neuronal activities. Similarly, we investigated how NMDA synaptic conductance affects the EF modulation effect on neuronal activity at the single-neuron level. Our results showed that when NMDA synaptic conductance is small, slow and fast dendritic oscillations, as well as somatic Na^+ discharges, are more likely to coexist under EF stimulation. An increase in NMDA synaptic conductance leads to more dendritic NMDA spikes within a single dendritic spike and also gives rise to somatic burst discharge. These findings emphasize the importance of neuronal electrophysiological properties in influencing the EF modulation effects on multi-timescale neuronal oscillations and highlight the challenges in optimizing parameters for electromagnetic stimulation in epilepsy treatment.

As experimental techniques improve, the influence of EF-induced dendritic polarization on dendrite activities has gained increasing attention,[24,37–39] such as its modulation effect on synaptic plasticity[37,38] and its impact on calcium channel activity.[23,40] These findings indicate that dendritic polarization can influence the neuronal input–output relationship by regulating local dendritic spikes. Differently, our study examines the EF modulation sensitivity when multiple dendrites generate NMDA spikes and Ca^{2+} spikes. We found that the dendritic spikes generated in multiple branches enhance the interaction among dendrites, leading to a more sensitive EF modulation effect as well as a nonlinear regulation effect that has not been extensively reported in previous studies.[24]

Currently, the two-compartment neuronal model is commonly used to study how an EF modulates neuronal activity from the point of view of dynamics.[32,33] These models typically describe the EF's spatial polarization effects through the coupling conductance between compartments. We also adopt the coupling conductance to depict the modulation effect of an EF on multi-timescale neuronal oscillations with a normal three-compartment model (Subsection 3.3). However, our results indicate that the coupling conductance cannot fully capture the input–output relationship of the biophysical model. Even if the three-compartment model could reproduce the coexistence of dendritic Ca^{2+} oscillations, NMDA oscillations, and somatic Na^+ discharges under EF stimulation, it cannot be used to explore the EF modulation mechanism on multi-timescale neuronal oscillations. By comparing the dendritic morphology between the three-compartment model and the layer 5 pyramidal neuron, we think that the loss of spatial dendritic distribution makes the three-compartment model fail to fully characterize the spatial EF-induced polarization, which results in higher stimulation thresholds for generating multi-timescale neuronal oscillations. Our simplified model with five apical dendrites demonstrates that the EF stimulation threshold for triggering dendritic spikes decreases with the increasing number of dendritic branches, which demonstrates our hypothesis. These results indicate that the dendritic morphology plays an important role in determining EF-induced polarization,[33,36] and the simplified three-compartment model needs another parameter to account for the EF-induced spatial polarization of a layer 5 pyramidal neuron.

The involvement of the EF in epileptiform phenomena has been highlighted in previous studies.[16] To investigate how the EF induces the generation of neuronal oscillations with multiple timescales from a dynamic perspective, we developed a modified three-compartment model with an independent EF sensitivity parameter. As shown in Fig. 8, the modified three-chamber model accurately represents the coexistence of dendritic Ca^{2+} oscillations, NMDA oscillations, and somatic Na^+ discharges under EF stimulation. Using singular perturbation analysis, we decomposed the model into three subsystems with distinct timescales, allowing us to explore the dynamic mechanism by which the EF modulates interactions between multi-timescale neuronal oscillations. When the synchronous activity of a neural population increases, the intensity of the endogenous electric field also increases. Under anodal EF stimulation, the basal dendritic and somatic depolarization sequentially triggers dendritic NMDA oscillations and somatic Na^+ oscillations via two subcritical Hopf bifurcations. Conversely, under cathodal EF stimulation, the increasing depolarization of the apical dendrite results in an SNIC bifurcation to trigger dendritic Ca^{2+} oscillations. Then these oscillations drive the basal dendrite to generate dendritic NMDA oscillations via a subcritical Hopf bifurcation. Ultimately, the combination of dendritic Ca^{2+} and NMDA oscillations induces somatic Na^+ discharge via a subcritical Hopf bifurcation. These results not only explain how a neuron transitions from a resting state to oscillation and from simple oscillation to compound oscillation from a dynamic perspective, but also demonstrate that the dendritic Ca^{2+} oscillation serves as the source for inducing multi-timescale neuronal oscillations. Moreover, our results suggest that inhibiting dendritic Ca^{2+} oscillations can effectively suppress epileptiform discharges.

In conclusion, this work not only elucidates the biophysical mechanisms behind multi-timescale compound oscillations in pyramidal neurons under EF stimulation but also offers new perspectives for understanding the modulation of neuronal activity in the context of epilepsy treatment. However, there are some limitations in our study. First, we only used a layer 5 pyramidal neuron to investigate how EFs modulate multi-timescale neuronal oscillations. It is necessary to use more neuronal models to verify our results in future work. Second, the hyperpolarization-activated ionic current

(I_h) plays a crucial role in determining EF-regulated influences, but it is not introduced into our neuronal model. Our previous study[41] showed that during cathodal stimulation, the existence of I_h would lead to a more pronounced sublinear dendritic integration, suggesting that a neuron with I_h requires stronger cathodal stimulation to trigger multi-timescale neuronal oscillations. In our future work, we will verify this hypothesis. Third, although the real EF in the brain is time-varying, we modeled it as a uniform EF in our study. The entrainment effect of time-varying EFs on multi-timescale neuronal oscillations should be investigated in future work. Generally speaking, these limitations do not influence the effectiveness of our results, which provides insight into how applied fields interact with multi-timescale neuronal oscillations.

Supplementary data

In the supporting information, we provided a detailed introduction to singular perturbation analysis.

Acknowledgement

Project supported by the National Natural Science Foundation of China (Grant Nos. 62571367, 62271348, and 62171312).

References

[1] Hui Y and Stephanie K 2019 *IBRO Reports* **7** 26
[2] Löscher W, Potschka H, Sisodiya S M, *et al.* 2020 *Pharmacol Review* **72** 606
[3] Schevon C, Weiss S, McKhann G and Vezzani A 2012 *Nat. Commun.* **3** 1060
[4] Stuart G J and Spruston N 2015 *Nat. Neurosci.* **18** 1713
[5] Payeur A, Jean-Claude B and Naud R 2019 *Current Opinion in Neurobiology* **58** 78
[6] Cressman J R, Ullah G, Ziburkus J, Schiff S J and Barreto E 2009 *J. Computa. Neurosci.* **26** 159
[7] Thomas M, Ranjith G, Radhakrishnan A and Arun Anirudhan V 2019 *Neuroscience* **423** 148
[8] Holt A B and Netoff T I 2013 *Exprimental Neurology* **244** 75
[9] Dallmer-Zerbe I, Jiruska P and Hlinka J 2023 *Epilepsia* **64** 2221
[10] Milton J G 2010 *Epilepsy and Behavior* **18** 33
[11] Tran-Van-Minh A, Cazé R D, Abrahamsson T, Cathala L, Gutkin B S and DiGregorio D A 2015 *Frontiers in Cellular Neuroscience* **9** 67
[12] Larkum M E, Wu J M, Duverdin S A and Gidon A 2022 *Neuroscience* **489** 15
[13] Zheng H, Zheng Z, Hu R, Xiao B, Wu Y, Yu F, Liu X, Li G and Deng L 2024 *Nat. Commun.* **15** 277
[14] Sivakumar S, Ghasemi M and Schachter S C 2022 *Pharmaceuticals* **15** 129
[15] Cain S M and Snutch T P 2010 *Epilepsia* **51** 11
[16] Chiang C C, Wei X L, Ananthakrishnan A K, Shivacharan R S, Gonzalez-Reyes L E, Zhang M and Durand D M 2018 *Sci. Rep.* **8** 1564
[17] Fourz T J and Wong M 2022 *Biomedical Journal* **45** 27
[18] Starnes K, Miller K and Wong-Kisiel L 2019 *Brain Sciences* **9** 283
[19] Hu B, Zhao J, Ao Y and Cai X Y 2025 *Nonlinear Dyn.* **113** 2711
[20] Qiu C, Shivacharan R S, Zhang M M and Durand D M 2015 *J. Neurosci.* **35** 15800
[21] Bikson M, Inoue M, Akiyama H, Deans J K, Fox J E, Miyakawa H and Jefferys J G 2004 *Journal of Physiology-London* **557** 175
[22] Krause M R, Vieira P G, Csorba B A, Pilly P K and Pack C C 2019 *Proc. Natl. Acad. Sci.* **116** 5747
[23] Yi G S, Wei X L, Wang J, Deng B and Che Y Q 2019 *Neural Network* **110** 8
[24] Fan Y Q, Wei X L, Lu M L, Wang J and Yi G S 2024 *Cognitive Neurodynamics* **18** 199
[25] Fan Y Q, Wei X L, Lu M L, Wang J and Yi G S 2023 *Sci. Rep.* **13** 16485
[26] Wei X L, Ren Z Y, Lu M L, Fan Y Q and Chang S Y 2024 *Chin. Phys. B* **33** 068702
[27] Zhang F, Lu M L and Wei X L 2025 *Nonlinear Dyn.* **113** 1685
[28] Augusto E and Gambino F 2019 *Frontiers in Molecular Neuroscience* **12** 238
[29] Larkum M E, Nevian T, Sandier M, Polsky A and Schiller J 2009 *Science* **325** 756
[30] Poleg-Polsky A 2015 *PLoS One* **10** e0140254
[31] Hines M L and Carnevale N T 1997 *Neural Comput.* **9** 1179
[32] Yi G S, Wang J, Wei X L, Tsang K M, Chan W L, Deng B and Han C X 2014 *J. Comput. Neurosci.* **36** 383
[33] Yi G S, Wang J, Wei X L, Chan W L and Deng B 2014 *PLoS One* **9** e97481
[34] Wang Z, Hu B, Zhou W, Xu M B and Wang D J 2023 *Chaos, Solitons and Fractals* **166** 113022
[35] Zhang M M, Ladas T P, Qiu C, Shivacharan R S, Gonzalez-Reyes L E and Durand D M 2014 *J. Neurosci.* **34** 1409
[36] Radman T, Ramos R L, Brumberg J C and Bikson M 2009 *Brain Stimulation* **2** 215
[37] Rahman A, Lafon B, Parra L C and Bikson M 2017 *Journal Physiology* **595** 3535
[38] Kronberg G, Bridi M, Abel T, Bikson M and Parra L C 2017 *Brain Stimulation* **10** 51
[39] Krongberg G, Rahman A, Sharma M, Bikson M and Parra L C 2020 *Brain Stimulation* **13** 287
[40] Kato I, Innami K, Sakuma K, Miyakawa H, Inoue M and Aonishi T 2019 *Brain Research Bulletin* **153** 202
[41] Fan Y Q, Wei X L, Yi G S, Lu M L and Wang J 2022 *Nonlinear Dyn.* **108** 4335